

# Examination of the adiabatic approximation for $(d, p)$ reactions

Yoshiki Chazono,<sup>1,\*</sup> Kazuki Yoshida,<sup>1</sup> and Kazuyuki Ogata<sup>1</sup>

<sup>1</sup>Research Center for Nuclear Physics (RCNP), Osaka University, Ibaraki 567-0047, Japan

(Dated: September 17, 2018)

**Background:** Deuteron-induced one-neutron transfer reactions have been used to extract single-particle properties of nuclei, and the adiabatic (AD) approximation is often used to simply treat the deuteron breakup states.

**Purpose:** The primary goal is to examine the validity of the AD approximation for the  $(d, p)$  reaction systematically. We clarify also the role of the closed channels often ignored in the description of breakup reactions.

**Methods:** We calculate the  $(d, p)$  cross sections with the continuum-discretized coupled-channels method (CDCC) for 128 reaction systems and compare the results with those obtained by the CDCC calculation with the AD approximation. Effect of the closed channels are investigated by ignoring them in CDCC.

**Results:** The AD approximation affects in general the  $(d, p)$  cross section by less than 20 %, but some exceptional (*nonadiabatic*) cases for which the AD approximation breaks down are found. The closed channels turn out to give significant effects on the cross section at deuteron energies less than about 10 MeV.

**Conclusions:** The use of the AD approximation in the description of the  $(d, p)$  reaction can be justified in many cases, with the uncertainty of less than about 20 %. The existence of some nonadiabatic cases nevertheless should be realized. The neglect of the closed channels without confirming the convergence of the CDCC result is not recommended.

PACS numbers: 24.10.-i, 24.10.Eq, 25.45.-z, 25.45.Hi

## I. INTRODUCTION

Nucleon transfer reactions have played a substantial role in extracting single-particle (s.p.) properties of nuclei. Deuteron-induced transfer reactions, that is,  $A(d, p)B$  and  $A(d, n)C$  processes, are particularly important because the s.p. information on B or C not only in the ground state (g.s.) but also in excited states can be studied. Furthermore, these reactions in inverse kinematics can be applied to studies of unstable nuclei; numbers of results have been reported in, e.g., Refs. [1–5]. In these studies, the adiabatic (AD) approximation [6, 7] was employed for describing the  $(p + n)$ -A three-body wave function with efficiently taking into account the breakup effect of deuteron; this framework is called adiabatic distorted-wave approximation (ADWA).

On the theoretical side, the reaction mechanism of the  $(d, N)$  reactions ( $N = p$  or  $n$ ) has intensively been studied with three-body reaction theories [8–12]. Nowadays the calculation with the Faddeev–Alt–Grassberger–Sandhas (FAGS) theory [13, 14] is feasible [15, 16] that gives the exact solution to the  $(d, N)$  cross section with a given three-body Hamiltonian; very recently, the role of the core excitation in  $(d, p)$  reactions has also been studied [17]. However, situation of the  $(d, N)$  reactions is still complicated; the energy dependence of the distorting potentials for  $p$  and  $n$ , as well as their nonlocality has been a matter of discussion [15, 16, 18–21]. In Refs. [18–21] a simple prescription for implementing these ingredients was proposed within the framework of ADWA. This prescription is very helpful to minimize the numerical tasks for evaluating properly  $(d, N)$  cross sections; its validity depends on, however, that of the AD approximation adopted.

In this study we systematically examine the AD approxi-

mation to the three-body scattering wave function in the initial channel of the  $A(d, p)B$  process. We employ the continuum-discretized coupled-channels method (CDCC) [22–24] as a three-body reaction model, and compare the resulting  $(d, p)$  cross sections with those calculated by CDCC with the AD approximation. For simplicity we neglect the intrinsic spin of each nucleon in the CDCC calculation; the zero-range approximation with the finite-range correction [12] is adopted in the calculation of the  $(d, p)$  transition matrix. Furthermore, we fix the energy used in evaluating  $p$ -A and  $n$ -A optical potentials at half of the incident deuteron energy; the effect of nonlocality of the potentials are not taken into account. We thus concentrate on the effect of the AD approximation of the  $d$ -A scattering wave on the  $(d, p)$  cross sections. It should be noted that, in Refs. [25–27], a numerical test for ADWA has been done for some reaction systems. In this study, we consider four target nuclei, four incident energies, four transferred angular momenta, and two possibilities of the neutron separation energy of the residual nucleus B; in total we consider 128 reaction systems. In addition to that, we investigate the effect of the closed channels (see Sec. III C) on the  $(d, p)$  cross sections. The closed channels are sometimes neglected in CDCC calculations [26] and can significantly affect reaction observables at low energies in particular [28].

The construction of this paper is as follows. In Sec. II we briefly describe the reaction model adopted. In Sec. III we first explain the numerical inputs and discuss the systematics of the validity of the AD approximation. The role of the closed channels is also clarified. Finally we give a summary in Sec IV.

## II. THEORETICAL FRAMEWORK

We adopt the three-body system consisting of  $p$ ,  $n$ , and the target nucleus A, shown in Fig. 1. The residual nucleus B

\*chazono@rcnp.osaka-u.ac.jp

in the final channel is assumed to be a bound state of the  $n$ - $A$  system. The post form of the transition matrix for the  $A(d, p)B$  process is given by

$$T_{\beta\alpha} = \langle \Phi_{\beta}^{(-)} | V_{pn} | \Psi_{\alpha}^{(+)} \rangle, \quad (1)$$

where  $V_{pn}$  is the interaction between  $p$  and  $n$ , and  $\Psi_{\alpha}^{(+)}$  is the exact three-body scattering wave function in the initial channel satisfying the Schrödinger equation

$$[H_{\alpha} - E]\Psi_{\alpha}^{(+)}(\mathbf{R}_{\alpha}, \mathbf{r}_{\alpha}) = 0 \quad (2)$$

with the outgoing boundary condition. The three-body Hamiltonian  $H_{\alpha}$  in Eq. (2) is written as

$$H_{\alpha} = T_{\mathbf{R}_{\alpha}} + U_p(r) + U_n(r_{\beta}) + h_{pn}, \quad (3)$$

where  $T_{\mathbf{R}_{\alpha}}$  is the kinetic energy operator regarding the coordinate  $\mathbf{R}_{\alpha}$ ,  $U_p$  and  $U_n$  are the proton and neutron distorting potentials by  $A$ , respectively, and  $h_{pn}$  is the internal Hamiltonian of the  $p$ - $n$  system. Definition of  $\Phi_{\beta}^{(-)}$  is given below.

We adopt CDCC to obtain  $\Psi_{\alpha}^{(+)}$ :

$$\Psi_{\alpha}^{(+)} = \sum_{i=0}^{i_{\max}} \phi_i(\mathbf{r}_{\alpha}) \chi_i^{(+)}(\mathbf{R}_{\alpha}), \quad (4)$$

where  $\phi_0$  is the deuteron bound-state wave function and  $\phi_i$  for  $i \neq 0$  denote discretized continuum states. The  $\phi_i$  satisfy

$$h_{pn}\phi_i(\mathbf{r}_{\alpha}) = \epsilon_i\phi_i(\mathbf{r}_{\alpha}) \quad (5)$$

with  $\epsilon_i$  being the eigenenergy of the  $p$ - $n$  system. Equation (4) means that the total wave function is expanded in terms of the set of the eigenstates of  $h_{pn}$ , which is assumed to form a complete set in the space relevant to the physics observables of interest. The expansion ‘‘coefficients’’ are denoted by  $\chi_i^{(+)}$  which physically represent the scattering waves between  $A$  and the  $p$ - $n$  system in the  $i$ th state. Although CDCC is not an exact theory for three-body scattering processes, its theoretical foundation is given in Refs. [29, 30] in connection

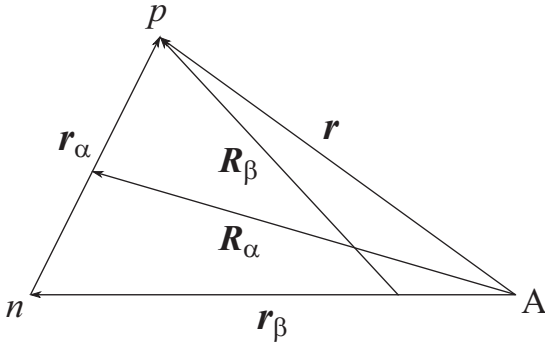


FIG. 1: Illustration of the three-body system.

with the distorted-wave Faddeev formalism [31], and thus can be regarded as a very good approximation to the FAGS theory [13, 14]. It should be noted that the striking difference between the results of CDCC and FAGS for low-energy deuteron breakup cross sections found in Ref. [26] was shown to be mainly because of the lack of the CDCC model space [28]. In Ref. [26], it was reported also that  $(d, p)$  cross sections obtained by CDCC somewhat deviate from those by FAGS at incident deuteron energies higher than about 40 MeV, which we do not discuss in this study. For further details of CDCC, readers are referred to Refs. [22–24]. To examine the AD approximation, we do not adopt the usual ADWA framework but make all  $\epsilon_i$  for  $i \neq 0$  equal to  $\epsilon_0$  in solving the CDCC equations, to minimize the model uncertainty. We call this calculation CDCC-AD in the following.

The three-body wave function  $\Phi_{\beta}^{(-)}$  in the final channel having the incoming boundary condition is a solution of

$$[H_{\beta} - E]\Phi_{\beta}^{(-)}(\mathbf{R}_{\beta}, \mathbf{r}_{\beta}) = 0, \quad (6)$$

$$H_{\beta} = T_{\mathbf{R}_{\beta}} + U_p^*(r) + h_{nA}, \quad (7)$$

where  $T_{\mathbf{R}_{\beta}}$  is the kinetic energy operator associated with  $\mathbf{R}_{\beta}$  and  $h_{nA}$  is the internal Hamiltonian of the  $n$ - $A$  bound system.

In the present study the three-body wave function of the final channel is approximated by

$$\Phi_{\beta}^{(-)} \approx \varphi_n(\mathbf{r}_{\beta})\psi_p^{(-)}(\mathbf{R}_{\beta}), \quad (8)$$

where  $\varphi_n$  is the neutron bound-state wave-function and  $\psi_p^{(-)}$  is the distorted wave for the outgoing proton. Because the purpose of the present study is to investigate the validity of the AD approximation to  $\Psi_{\alpha}^{(+)}$ , we restrict ourselves not to discuss the breakup effect in the final channel.

The transfer reaction is described by a one-step process with the zero-range approximation to  $V_{pn}\phi_i$ ; the finite range correction following Ref. [12] is made. In some figures shown in Sec. III B, we decompose the transition matrix of Eq. (1) into the elastic transfer (ET) part  $T_{\beta\alpha}^{\text{ET}}$  and the breakup transfer (BT) part  $T_{\beta\alpha}^{\text{BT}}$  as

$$T_{\beta\alpha} = T_{\beta\alpha}^{\text{ET}} + T_{\beta\alpha}^{\text{BT}}, \quad (9)$$

$$T_{\beta\alpha}^{\text{ET}} \equiv \langle \Phi_{\beta}^{(-)} | V_{pn} | \phi_0(\mathbf{r}_{\alpha}) \chi_0^{(+)}(\mathbf{R}_{\alpha}) \rangle, \quad (10)$$

$$T_{\beta\alpha}^{\text{BT}} \equiv \langle \Phi_{\beta}^{(-)} | V_{pn} | \sum_{i \neq 0}^{i_{\max}} \phi_i(\mathbf{r}_{\alpha}) \chi_i^{(+)}(\mathbf{R}_{\alpha}) \rangle. \quad (11)$$

The cross section calculated with replacing  $T_{\beta\alpha}$  with  $T_{\beta\alpha}^{\text{ET}}$  ( $T_{\beta\alpha}^{\text{BT}}$ ) is designated as the ET (BT) cross section.

### III. RESULTS AND DISCUSSION

#### A. Numerical inputs

We consider four target nuclei having the atomic number  $Z$  and the mass number  $A$  of  $(Z, A) = (10, 20), (20, 40),$

(40, 100), and (80, 200), which we call in the following  $^{20}\text{Ne}$ ,  $^{40}\text{Ca}$ ,  $^{100}\text{Zr}$ , and  $^{200}\text{Hg}$ , respectively. These nuclei are assumed to have a fictitious s.p. structure so that a neutron is transferred to  $\ell_f = 0, 1, 2,$  or  $3$  orbits in the residual nucleus B, where  $\ell_f$  is the orbital angular momentum of the transferred neutron. The principal quantum number of the neutron starting from 0 is determined with the assumption that the target nucleus A has a naïve shell structure; in Table I we list the s.p. orbit for the neutron transferred to nucleus A. Furthermore, the neutron separation energy  $S_n$  of B is supposed to be 0.1 MeV or 8.0 MeV. The Bohr-Mottelson s.p. potential [32] is used to calculate the neutron bound-state wave function.

TABLE I: Single-particle orbit for the transferred neutron.

Target	$ell_f$			
	0	1	2	3
$^{20}\text{Ne}$	$1s_{1/2}$	$1p_{3/2}$	$0d_{5/2}$	$0f_{7/2}$
$^{40}\text{Ca}$	$2s_{1/2}$	$1p_{3/2}$	$1d_{5/2}$	$0f_{7/2}$
$^{100}\text{Zr}$	$2s_{1/2}$	$2p_{3/2}$	$1d_{5/2}$	$1f_{7/2}$
$^{200}\text{Hg}$	$3s_{1/2}$	$3p_{3/2}$	$2d_{5/2}$	$1f_{5/2}$

The deuteron incident energy  $E_d$  is taken to be 5, 10, 20, and 40 MeV. We adopt the Koning-Delaroche (KD) [33] nucleon optical potential as  $U_p$  and  $U_n$ , and the one-range Gaussian interaction [34] is employed as  $V_{pn}$ . The  $p$ - $n$  discretized continuum states of the  $s$ - and  $d$ -waves, with  $k_{\text{max}} = 2.0 \text{ fm}^{-1}$  and  $\Delta_k = 0.04 \text{ fm}^{-1}$ , are included in CDCC, where  $k_{\text{max}}$  is the maximum  $p$ - $n$  linear momentum (in the unit of  $\hbar$ ) and  $\Delta_k$  is the size of the momentum bin. The CDCC equations are integrated up to  $R_\alpha = 20 \text{ fm}$  with the increment of 0.1 fm; the Coulomb breakup is ignored in this study.

The distorted wave  $\psi_p^{(-)}$  for the outgoing proton is calculated with the KD potential. The integration of the transition matrix is taken up to 150 and 40 fm for  $S_n = 0.1$  and 8 MeV, respectively.

## B. Validity of the adiabatic approximation

In table II we show the adiabatic factor  $S_{\text{AD}}$  determined so as to minimize

$$\chi^2(S_{\text{AD}}) \equiv \int \left[ \left( \frac{d\sigma}{d\Omega} - S_{\text{AD}} \frac{d\sigma_{\text{AD}}}{d\Omega} \right) / \left( \frac{d\sigma}{d\Omega} \right) \right]^2 \times \Theta \left( \frac{d\sigma}{d\Omega} - \frac{1}{2} \frac{d\sigma^{\text{max}}}{d\Omega} \right) d\theta_{\text{cm}}, \quad (12)$$

where  $d\sigma/d\Omega$  and  $d\sigma_{\text{AD}}/d\Omega$  are the  $(d, p)$  differential cross sections calculated with CDCC and CDCC-AD, respectively,  $\Theta$  is the step function, and  $d\sigma^{\text{max}}/d\Omega$  is the maximum value of  $d\sigma/d\Omega$ . It should be noted that in the integration in Eq. (12) we ignore the weighting factor  $\sin \theta$ , where  $\theta$  is the scattering angle of the outgoing proton in the center-of-mass (c.m.) frame, as in the standard  $\chi^2$ -fitting procedure for the angular distribution.

TABLE II: Adiabatic factor  $S_{\text{AD}}$ . The superscripts \*1, \*2, and \*3 indicate the cases in which the AD approximation does not work. See the text for details.

Target	$ell_f = 0$							
	Energy ( $S_n = 0.1 \text{ MeV}$ )				Energy ( $S_n = 8 \text{ MeV}$ )			
	5	10	20	40	5	10	20	40
$^{20}\text{Ne}$	0.71*3	0.89	1.32	1.25	0.90	0.93	0.88	0.74
$^{40}\text{Ca}$	1.08*3	1.21	2.01*2	1.44*2	0.78	0.77	0.78	0.87
$^{100}\text{Zr}$	0.96	1.11	1.83*2	1.67*2	0.87*1	0.87	0.68	1.10
$^{200}\text{Hg}$	1.00	0.94	1.21	1.29	1.06*1	0.88	0.66	1.24

Target	$ell_f = 1$							
	Energy ( $S_n = 0.1 \text{ MeV}$ )				Energy ( $S_n = 8 \text{ MeV}$ )			
	5	10	20	40	5	10	20	40
$^{20}\text{Ne}$	0.94	1.00	0.99	0.92	0.84	0.83	0.83	0.91
$^{40}\text{Ca}$	0.94	0.80	0.87	1.15	0.81*1	0.80	0.93	0.85
$^{100}\text{Zr}$	0.96	0.90	0.74	2.00*2	0.96	0.80	0.85	1.02
$^{200}\text{Hg}$	1.00	0.93	1.06	1.56*2	0.94*1	0.75*1	0.74	0.92

Target	$ell_f = 2$							
	Energy ( $S_n = 0.1 \text{ MeV}$ )				Energy ( $S_n = 8 \text{ MeV}$ )			
	5	10	20	40	5	10	20	40
$^{20}\text{Ne}$	0.92	0.82	0.88	0.98	0.95	0.94	0.92	0.90
$^{40}\text{Ca}$	0.93	0.83	0.92	0.92	0.66*1	0.77*1	0.84	0.90
$^{100}\text{Zr}$	0.97	0.85	0.84	0.92	0.83*1	0.80*1	0.77	0.86
$^{200}\text{Hg}$	1.00	0.93	0.86	0.97	1.04*1	0.76	0.82	0.88

Target	$ell_f = 3$							
	Energy ( $S_n = 0.1 \text{ MeV}$ )				Energy ( $S_n = 8 \text{ MeV}$ )			
	5	10	20	40	5	10	20	40
$^{20}\text{Ne}$	0.89	0.92	0.92	0.85	0.74	0.78	0.85	0.88
$^{40}\text{Ca}$	0.90	0.83	0.83	0.89	0.87*1	0.86*1	0.92	0.98
$^{100}\text{Zr}$	0.98	0.86	0.82	0.86	0.84*1	0.72*1	0.81	0.93
$^{200}\text{Hg}$	1.00	0.93	0.82	0.83	0.99	0.75*1	0.74	0.74

One sees from Table II that  $S_{\text{AD}}$  does not largely deviate from unity in general; the AD approximation affects the  $(d, p)$  cross section by less than 20 % and by about 35 % at most. In some exceptional cases, however,  $S_{\text{AD}}$  has a very large value, meaning the clear breakdown of the AD approximation. Furthermore, there are some cases in which  $S_{\text{AD}}$  is quite close to unity but the angular distribution of the transfer cross section is severely affected by the AD approximation. The angular distribution of the  $(d, p)$  cross sections for the 128 systems calculated with CDCC and CDCC-AD can be found in the Addendum provided as supplemental material [35].

Before discussing the *nonadiabatic* cases one by one, let us first see typical cases in which the AD approximation works well. Figure 2(a) shows the result for  $^{100}\text{Zr}(d, p)^{101}\text{Zr}(2s_{1/2})$  at  $E_d = 5 \text{ MeV}$  with  $S_n = 0.1 \text{ MeV}$ . The solid and dashed

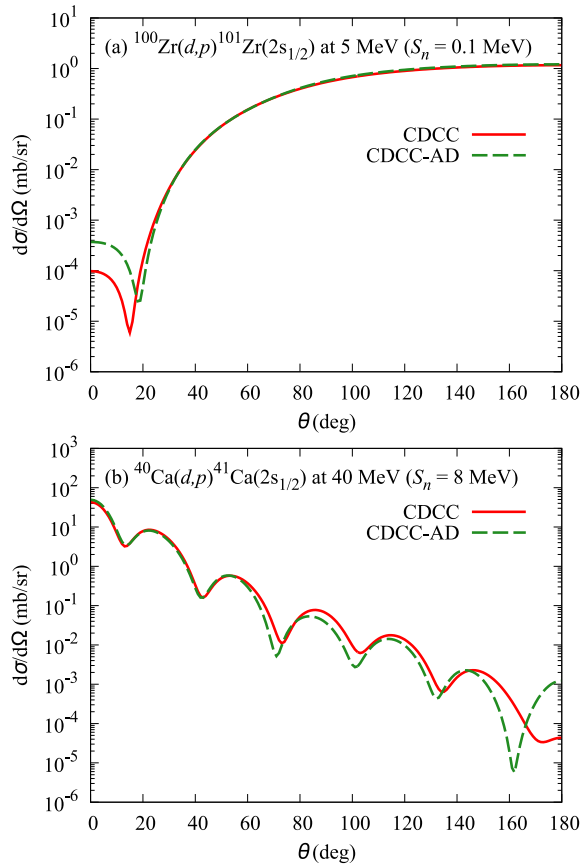


FIG. 2: (Color online) Angular distributions of the  $(d, p)$  cross sections calculated with CDCC (solid lines) and CDCC-AD (dashed lines) for (a)  $^{100}\text{Zr}(d, p)^{101}\text{Zr}(2s_{1/2})$  at  $E_d = 5$  MeV with  $S_n = 0.1$  MeV and (b)  $^{40}\text{Ca}(d, p)^{41}\text{Ca}(2s_{1/2})$  at  $E_d = 40$  MeV with  $S_n = 8$  MeV.

lines show the results of CDCC and CDCC-AD, respectively. When  $E_d$  is much smaller than the Coulomb barrier height, as is well known, the angular distribution is dictated by the property of the Coulomb trajectory [36] and has a backward-peak structure; this is called Coulomb-dominated transfer angular distributions. In the case shown in Fig. 2(a),  $S_{\text{AD}}$  is 0.96 and the reaction can be regarded as adiabatic. At the first look, it seems to be strange that the AD approximation works at such low incident energy. The reason for this is given below in comparison with the result for the  $S_n = 8$  MeV case.

In Fig. 2(b) we show the result for  $^{40}\text{Ca}(d, p)^{41}\text{Ca}(2s_{1/2})$  at 40 MeV and  $S_n = 8$  MeV. The incident energy is well above the Coulomb barrier and the angular distribution shows the diffraction pattern. The AD factor in this case is 0.87, which shows the success of the AD approximation with about 10 % error. This is quite natural because as  $E_d$  increases the deuteron internal motion becomes slow relative to the motion of the c.m. of the deuteron, resulting in the validness of the AD approximation. In general, this is the case for  $E_d \geq 20$  MeV with  $S_n = 8$  MeV. One should keep it in mind, however, that there exists not so large but finite differ-

ence coming from the use of the AD approximation.

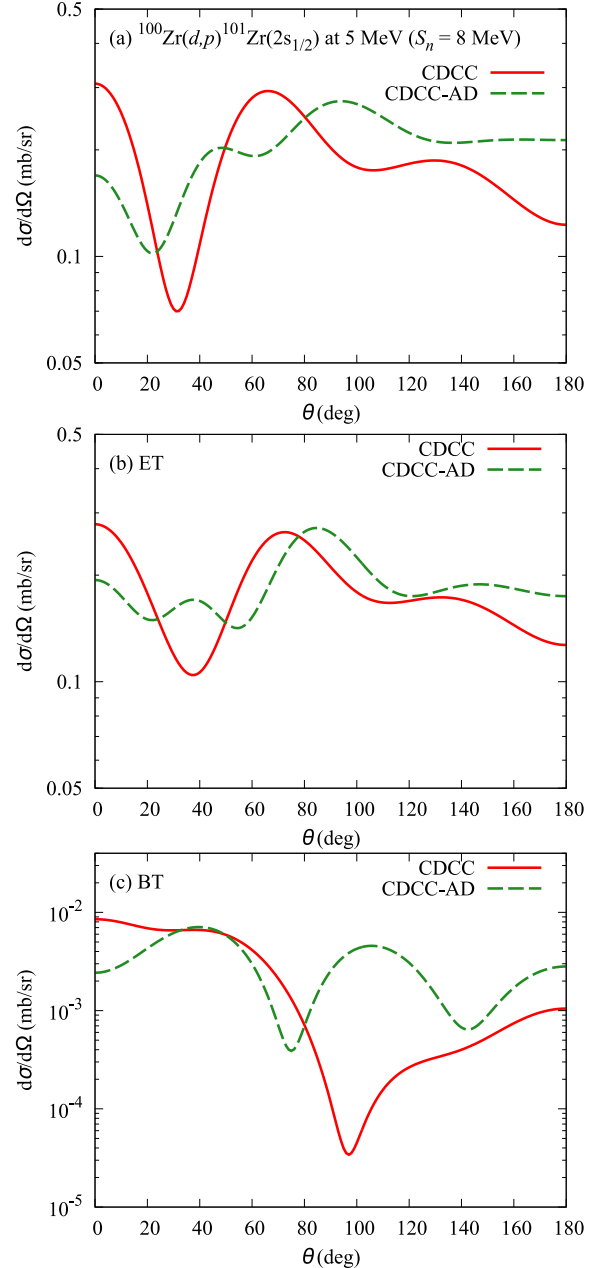


FIG. 3: (Color online) (a) Same as in Fig. 2 but for  $S_n = 8$  MeV; (b) ET cross section and (c) BT cross section.

At lower energy, the validity of the AD approximation becomes questionable. Although  $S_{\text{AD}}$  does not deviate from unity very much, the  $(d, p)$  angular distribution seriously suffers from the AD approximation for  $E_d \leq 10$  MeV and  $S_n = 8$  MeV; we put \*1 in Table II to specify the systems for which this is the case. As an typical example, the  $(d, p)$  cross section for  $^{100}\text{Zr}(d, p)^{101}\text{Zr}(2s_{1/2})$  at  $E_d = 5$  MeV with  $S_n = 8$  MeV is shown in Fig. 3(a). Clearly, the AD approximation fails to reproduce the result of CDCC. In Figs. 3(b) and 3(c), we show the cross sections of the ET and BT, re-

spectively. Despite the interference between the ET and BT amplitude is not negligible, one may see that the difference between the two lines in Fig. 3(a) mainly comes from that in the ET process. This suggests that the AD approximation cannot treat the coupling of the breakup channels to the elastic channel, that is, the so-called back-coupling. The difference between the two lines is very large also in the BT cross section. Nevertheless, the BT process itself is not so important because of its small contribution for the reaction systems indicated by \*1 in Table II.

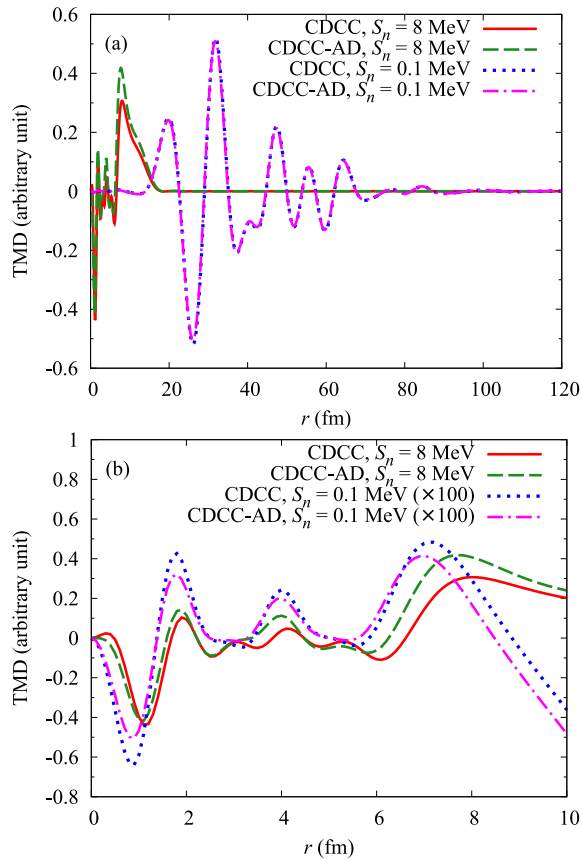


FIG. 4: (Color online) (a) TMDs for the ET part of the cross section at  $40^\circ$  for  $^{100}\text{Zr}(d, p)^{101}\text{Zr}(2s_{1/2})$  at  $E_d = 5$  MeV. The solid (dashed) and dotted (dash-dotted) lines show the results with CDCC (CDCC-AD) for  $S_n = 8$  and  $0.1$  MeV, respectively. (b) Enlarged view of (a) for  $r \leq 10$  fm; the dotted and dash-dotted lines are multiplied by 100.

We discuss here the effect of  $S_n$ , which is the only difference in the reaction systems shown in Figs. 2(a) and 3(a), on the validity of the AD approximation. To see the role of  $S_n$  in more detail, we show in Fig. 4 the transition matrix density (TMD) originally proposed in Ref. [37] as a weighting function for evaluating the mean density of the  $(p, 2p)$  knockout reactions. The TMD can be interpreted as a spatial distribution of the cross section; see Refs. [37, 38] for details. The solid (dotted) and dashed (dash-dotted) lines in Fig. 4(a) show the TMDs for the ET cross section at  $\theta = 40^\circ$  calculated with CDCC and CDCC-AD, respectively, for  $S_n = 8$  MeV

( $0.1$  MeV). One sees that the TMD for  $S_n = 0.1$  MeV distributes from about  $15$  fm to  $80$  fm. In this region the partial waves of  $\Psi_\alpha^{(+)}$  for lower angular momenta between A and the c.m. of the  $p$ - $n$  system, which are distorted by  $U_p$  and  $U_n$ , have only a small contribution to  $\Psi_\alpha^{(+)}$ . In other words, the incident-wave part of  $\Psi_\alpha^{(+)}$  is dominant there. The use of the AD approximation therefore makes no difference in the ET amplitude. In fact, the breakup effect itself is found to be negligibly small, which trivially results in the tiny contribution of the BT process. This is why CDCC-AD successfully reproduces the result of CDCC for the reaction shown in Fig. 2(a). On the other hand, the TMD distributes below about  $15$  fm when  $S_n = 8$  MeV. In that region, the nuclear distortion including the back-coupling effect is significant. As mentioned, because of the low incident energy, the breakup effect cannot be treated accurately by the AD approximation.

As mentioned above, there is no difference in  $\Psi_\alpha^{(+)}$  for Fig. 2(a) and Fig. 3(a). What classifies the validity of the AD approximation is therefore the region where the reaction takes place. If the nuclear interior and surface regions are important, the AD approximation fails at low incident energies. If only the tail (asymptotic) region is important, the AD approximation works well even at low incident energies. In Fig. 4(b) the results for  $r \leq 10$  fm are shown; those for  $S_n = 0.1$  MeV are multiplied by 100. One may see the difference coming from the AD approximation indeed exists also for  $S_n = 0.1$  MeV. As mentioned, however, this region does not have a meaningful contribution to the cross section, resulting in the success of CDCC-AD.

Next we discuss the cases for which  $S_{AD}$  is significantly large; we put \*2 in Table II for them. Figure 5(a) shows the result for  $^{40}\text{Ca}(d, p)^{41}\text{Ca}(2s_{1/2})$  at  $40$  MeV with  $S_n = 0.1$  MeV, and Figs. 5(b) and 5(c) show the corresponding ET and BT cross sections, respectively. In this case, the result of CDCC-AD undershoots that of CDCC for the BT part, whereas the two calculations give almost the same result for the ET cross section except at very backward angles. Thus, in some cases for  $S_n = 0.1$  MeV and at relatively high incident energies, the AD approximation fails to describe the breakup property of deuteron in the  $(d, p)$  process. In consequence of this, the absolute value of the cross section calculated with CDCC-AD significantly smaller than that of CDCC.

It is well known that the AD approximation tends to overshoot the breakup cross section of the projectile, since the AD approximation makes all the  $p$ - $n$  continuum states degenerate to the g.s. of deuteron, and thus makes the coupling between the deuteron g.s. and its breakup states effectively stronger. In fact, the deuteron elastic breakup cross section  $\sigma_{EB}$  calculated with CDCC-AD is  $107$  mb and that with CDCC is  $73$  mb. On the other hand, the result of CDCC-AD is smaller than that of CDCC for the BT cross section as mentioned above. To see this in more detail, we show in Fig. 6 the TMD for the BT cross section corresponding to  $\theta = 0^\circ$ . In the tail region, the amplitude of the CDCC-AD is larger than that of CDCC, reflecting mainly the amplitudes of the deuteron scattering wave function in the breakup channels. This is consistent with the aforementioned results of  $\sigma_{EB}$ . On the other hand, in the sur-

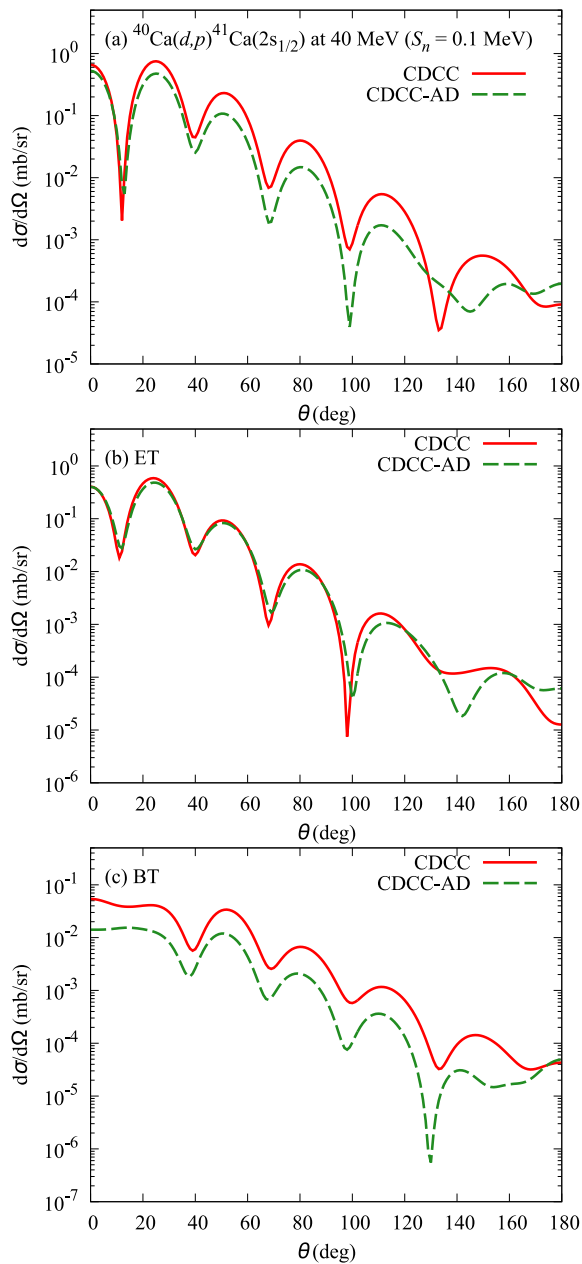


FIG. 5: (Color online) Same as in Fig. 3 but for  $^{40}\text{Ca}(d,p)^{41}\text{Ca}(2s_{1/2})$  at  $E_d = 40$  MeV with  $S_n = 0.1$  MeV.

face region around 7 fm, the result of CDCC (the solid line) has a larger positive value than that of CDCC-AD (the dashed line). Since the integrated value of the TMD is proportional to the cross section, the larger BT cross section of CDCC shown in Fig. 5(c) is due to the behavior of the solid line in Fig. 6 around 7 fm. It is, however, difficult to pin down the reason for this internal behavior, mainly because of the complicated coupled-channel effects.

Finally, we discuss the cases in which  $S_n = 0.1$  MeV and the result of CDCC-AD deviates from that of CDCC, even though  $S_{AD} \sim 1$ ; we put \*3 for them in Table II. The

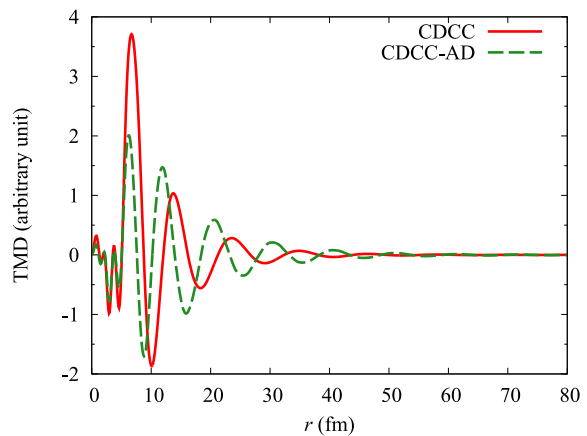


FIG. 6: (Color online) TMD for the BT cross section in Fig. 5(c) at  $0^\circ$ .

$(d,p)$  cross sections of  $^{40}\text{Ca}(d,p)^{41}\text{Ca}(2s_{1/2})$  at 5 MeV with  $S_n = 0.1$  MeV are shown in Fig. 7, as in Fig. 3. The shape of the cross section of CDCC-AD is somewhat different from that of CDCC, which is attributed to the difference in the BT cross sections. One of the important characteristics of this reaction system is the relation between  $E_d$  and the Coulomb barrier height  $V_{CB}$ . When  $E_d \ll V_{CB}$ , the Coulomb-dominated transfer angular distributions are observed, whereas the diffraction pattern develops when  $E_d > V_{CB}$  [36]. There is a window for  $E_d$  between these two conditions, that is,  $E_d \sim V_{CB}$ . In this region, the shape of the cross section starts changing from the Coulomb-dominated distribution to the diffraction pattern. The balance between  $E_d$  and  $V_{CB}$  is thus crucially important there. In CDCC, when the incident deuteron breaks up, the energy of the c.m. motion of the  $p$ - $n$  system decreases following the energy conservation of the three-body system. When  $E_d \sim V_{CB}$ , the  $p$ - $n$  c.m. energy in the breakup channels goes below  $V_{CB}$ , and the BT hardly contributes to the  $(d,p)$  cross section because of the Coulomb barrier. On the contrary, the AD approximation ignores the energy conservation and the penetrability of the scattering wave in breakup channels is the same as in the incident channel. As a result, the BT cross section is significantly overestimated by the CDCC-AD calculation. This is the case when  $E_d \sim V_{CB}$  and  $S_n = 0.1$  MeV; in fact, a similar result is obtained for  $^{200}\text{Hg}(d,p)^{201}\text{Hg}(3s_{1/2})$  around 15 MeV with  $S_n = 0.1$  MeV. When  $S_n$  is large, say, 8 MeV, the contribution of the BT becomes less important and the validity of the AD approximation mainly relies on the accurate description of the ET process as mentioned above.

Thus far we have discussed the validity of the AD approximation with respect to  $E_d$ ,  $S_n$ , and target nuclei. As for the trend in  $\ell_f$ , one can conclude from Table II that when  $S_n = 8$  MeV the selectivity of  $\ell_f$  is weak and  $E_d$  dictates the accuracy of the AD approximation. On the other hand, for  $S_n = 0.1$  MeV almost all the nonadiabatic cases are found when  $\ell_f = 0$ ; this may be related to the halo structure of the  $n$ -A system.

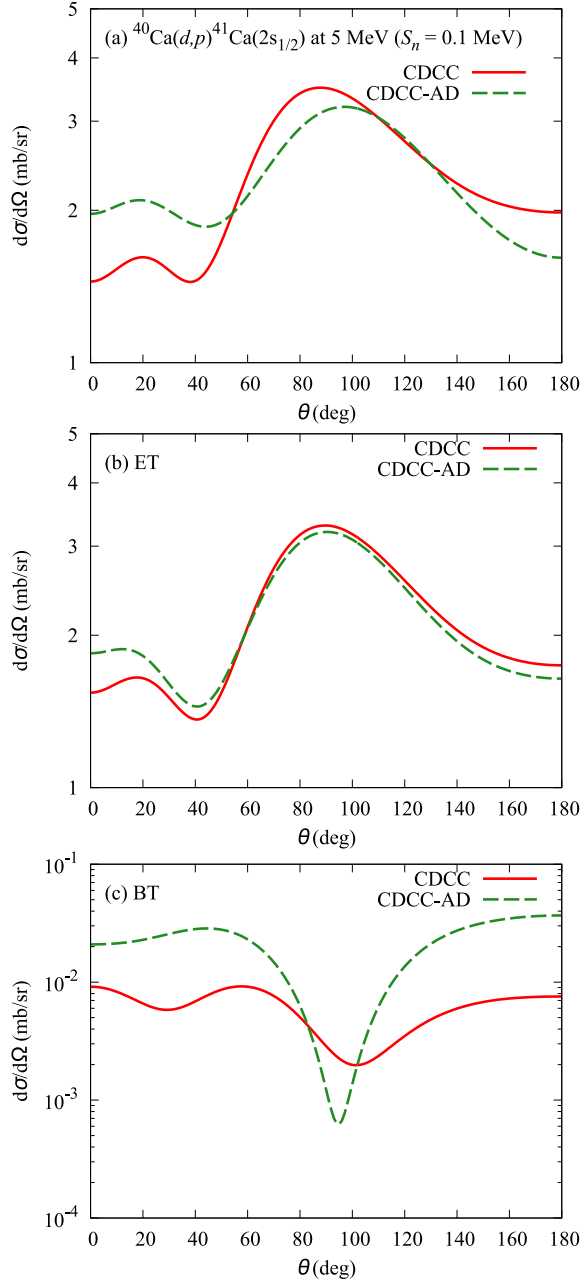


FIG. 7: (Color online) Same as in Fig. 3 but for  $^{40}\text{Ca}(d,p)^{41}\text{Ca}(2s_{1/2})$  at  $E_d = 5$  MeV with  $S_n = 0.1$  MeV.

### C. Effect of the closed channel

In our CDCC calculation, as mentioned, the maximum  $p$ - $n$  linear momentum  $k_{\max}$  is taken to be  $2.0 \text{ fm}^{-1}$ . In some studies, however,  $k_{\max}$  is determined by

$$\frac{\hbar^2 k_{\max}^2}{2\mu_{pn}} = E_0, \quad (13)$$

where  $\mu_{pn}$  is the reduced mass of the  $p$ - $n$  system and  $E_0$  is the deuteron incident energy in the c.m. system. In other

TABLE III: Values of  $S_{\text{OP}}$ . The superscript  $\dagger$  represents the cases in which  $S_{\text{OP}}$  does not deviate much from unity but the angular distribution is severely affected by the neglect of the closed channels.

$ell_f = 0$								
	Energy ( $S_n = 0.1$ MeV)				Energy ( $S_n = 8$ MeV)			
Target	5	10	20	40	5	10	20	40
$^{20}\text{Ne}$	1.00	1.09	1.16	1.00	0.85	1.04	1.10	0.91
$^{40}\text{Ca}$	1.27	1.39	1.25	0.95	0.58	0.92	1.04	0.92
$^{100}\text{Zr}$	1.00	1.18 $^\dagger$	1.13	0.94	0.89 $^\dagger$	1.02	0.84	0.93
$^{200}\text{Hg}$	1.00	0.99	0.94 $^\dagger$	0.94	1.08 $^\dagger$	0.84 $^\dagger$	0.89	0.96
$ell_f = 1$								
	Energy ( $S_n = 0.1$ MeV)				Energy ( $S_n = 8$ MeV)			
Target	5	10	20	40	5	10	20	40
$^{20}\text{Ne}$	1.13	1.07	1.02	0.97	0.90	1.04	1.00	0.96
$^{40}\text{Ca}$	1.19 $^\dagger$	0.99	0.95	0.99	0.62	0.88	0.97	0.97
$^{100}\text{Zr}$	1.00	1.02 $^\dagger$	0.91	0.95	0.69	0.88	0.89	0.98
$^{200}\text{Hg}$	1.00	0.99	0.98	0.95	0.94	0.72	0.89	0.98
$ell_f = 2$								
	Energy ( $S_n = 0.1$ MeV)				Energy ( $S_n = 8$ MeV)			
Target	5	10	20	40	5	10	20	40
$^{20}\text{Ne}$	1.04	1.02	0.95	1.00	0.79	0.91	0.93	1.00
$^{40}\text{Ca}$	1.06 $^\dagger$	0.96	0.96	0.97	0.79	0.91	0.94	0.98
$^{100}\text{Zr}$	1.01	0.96	0.98	0.95	0.92 $^\dagger$	0.94	0.90	1.00
$^{200}\text{Hg}$	1.00	0.99	0.95	0.96	1.05	0.89 $^\dagger$	0.90	1.00
$ell_f = 3$								
	Energy ( $S_n = 0.1$ MeV)				Energy ( $S_n = 8$ MeV)			
Target	5	10	20	40	5	10	20	40
$^{20}\text{Ne}$	0.93 $^\dagger$	0.96	0.98	0.99	1.13 $^\dagger$	1.01	1.02	1.00
$^{40}\text{Ca}$	1.07 $^\dagger$	0.92	0.96	0.98	0.69	0.77	0.92	1.00
$^{100}\text{Zr}$	1.01	0.97	0.94	0.98	0.80 $^\dagger$	0.71	0.89	0.99
$^{200}\text{Hg}$	1.00	0.99	0.96	1.00	1.00	0.98 $^\dagger$	0.90	1.00

words, the so-called closed channels are sometimes neglected. Recently, it was found that the inclusion of the closed channels in CDCC is crucial for accurately describing the deuteron breakup cross sections at low incident energies [28].

To see the importance of the closed channels for the  $(d,p)$  processes, we show in Table III the factor  $S_{\text{OP}}$  defined in the same way as for  $S_{\text{AD}}$  but with  $d\sigma_{\text{AD}}/d\Omega$  in Eq. (12) replaced with  $d\sigma_{\text{OP}}/d\Omega$ ;  $d\sigma_{\text{OP}}/d\Omega$  is the result of CDCC with  $k_{\max}$  determined by Eq. (13). As expected, for  $E_d \geq 20$  MeV the closed channels have no significant effect, resulting in  $S_{\text{OP}} \sim 1$ . However, in some cases the neglect of the closed channels affects the result by more than 10% even in that energy region. At lower energy, the effect of the closed channels can be very large, for  $S_n = 8$  MeV in particular. Furthermore, for the reaction systems indicated by  $\dagger$  in Table III, neglect of

the closed channels significantly changes the angular distribution, even though  $S_{OP}$  does not differ from unity. Figure 8 shows a typical example for those cases.

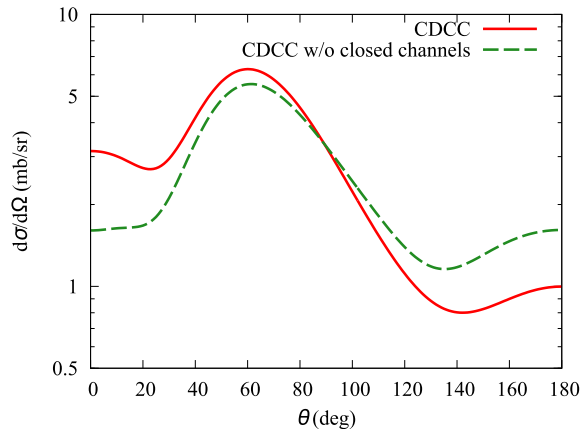


FIG. 8: (Color online) Angular distributions of the  $(d, p)$  cross sections for  $^{20}\text{Ne}(d, p)^{21}\text{Ne}(0f_{7/2})$  at  $E_d = 5$  MeV with  $S_n = 8$  MeV. The solid and dashed lines show the results of CDCC with and without the closed channels, respectively.

By taking a closer look at Table III, one may find that the tendency of  $S_{OP}$  is quite nontrivial. For instance, when  $\ell_f = 0$ ,  $S_n = 0.1$  MeV, and  $E_d = 5$  MeV,  $S_{OP}$  significantly deviates from unity only for  $^{40}\text{Ca}$ . In Fig. 9 we show the results of comparison for  $^{20}\text{Ne}$ ,  $^{40}\text{Ca}$ , and  $^{100}\text{Zr}$ .

One sees that a strikingly large effect of the closed channels appears when  $E_d \sim V_{CB}$ , as in the \*3 cases mentioned in Sec. III B. For  $\ell_f \neq 0$ , however, this seems not to be the case. Thus, we conclude that it is difficult to see *a priori* the role of the closed channels. We thus conclude that the use of Eq. (13) is not recommended;  $k_{\text{max}}$  must be determined so as to make the physics observables calculated with CDCC converged. Comparison for all the reaction systems as in Fig. 8 can be found in the addendum provided as supplemental material [35].

#### IV. SUMMARY

We have examined the validity of the adiabatic (AD) approximation to the deuteron-target three-body wave function in the calculation of the cross section of the  $(d, p)$  process for 128 reaction systems. For this purpose, results of CDCC that explicitly treat the breakup channels are compared with those of CDCC with the AD approximation (CDCC-AD). The typical error due to the AD approximation is found to be less than 20 % and around 35 % at most. However, there are three exceptional cases in which the AD approximation does not work.

First, when the deuteron incident energy  $E_d$  is less than 10 MeV and the neutron separation energy  $S_n$  in the residual nucleus is 8 MeV, the AD approximation cannot describe the  $(d, p)$  angular distribution calculated by CDCC, mainly because of the failure in describing the elastic transfer process.

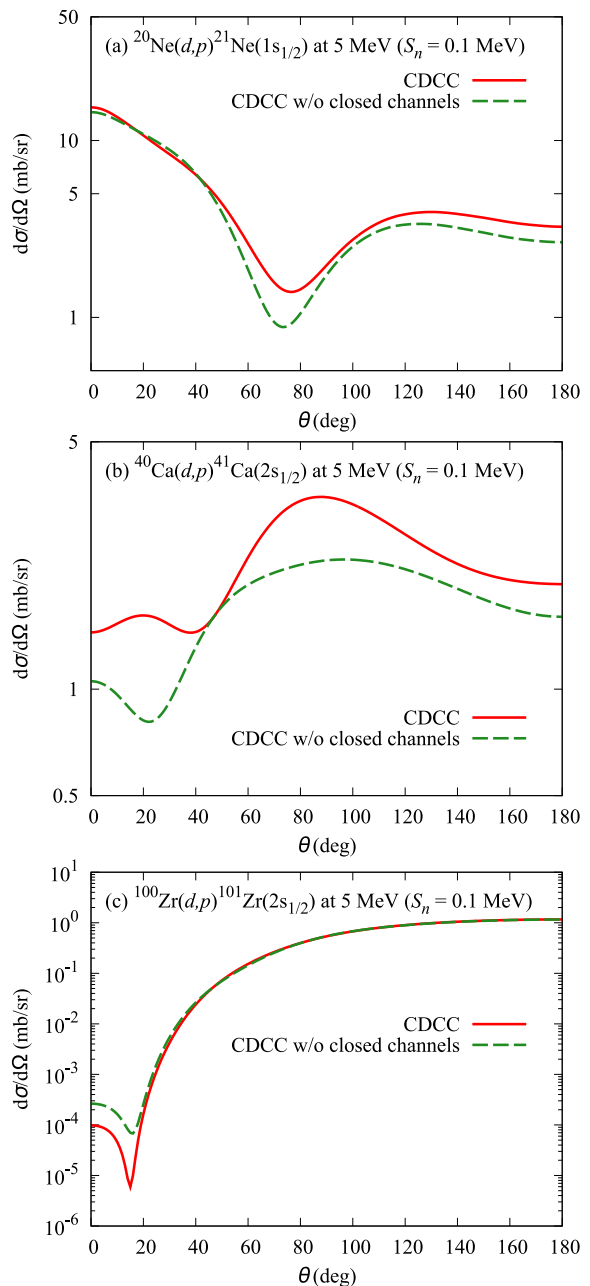


FIG. 9: (Color online) Same as in Fig. 8 but for (a)  $^{20}\text{Ne}(d, p)^{21}\text{Ne}(1s_{1/2})$ , (b)  $^{40}\text{Ca}(d, p)^{41}\text{Ca}(2s_{1/2})$ , and (c)  $^{100}\text{Zr}(d, p)^{101}\text{Zr}(2s_{1/2})$ , at  $E_d = 5$  MeV with  $S_n = 0.1$  MeV.

This will be natural because the assumption of the AD approximation, that is, the assumption that the internal motion of deuteron is much slower than that of the c.m. of deuteron, does not hold. In this case, however, if an appropriate optical potential that can describe the deuteron elastic channel is provided, the  $(d, p)$  process does not suffer from the deuteron breakup effect.

Second, for some reaction systems in which  $E_d \geq 20$  MeV and  $S_n = 0.1$  MeV, the result of CDCC-AD is significantly

smaller than that of CDCC. We found that this is due to the undershooting of the breakup transfer contribution by the AD approximation. It should be noted that the AD approximation overshoots the deuteron breakup cross section, because it enhances the breakup probability of deuteron in general. The effect due to the AD approximation on the breakup transfer (BT) process is opposite to it and will be a consequence of complicated coupled-channel effects.

Third, when  $E_d$  is close to the Coulomb barrier energy and  $S_n = 0.1$  MeV, the behavior of the BT process cannot be properly described by the AD approximation, because it violates the energy conservation of the three-body system; the energy of the c.m. of the  $p$ - $n$  system does not change even after breakup and can penetrate the Coulomb barrier as in the elastic channel.

We have investigated also the effect of the closed channels. For  $E_d \leq 20$  MeV, the neglect of the closed channels can seriously affect the result, for  $S_n = 8$  MeV in particular. However, there seems no clear threshold above which the closed channels can be neglected. It will be recommended that the convergence of the CDCC model space with respect to  $k_{\max}$  should always be confirmed, as for other quantities such as

$l_{\max}$  and  $\Delta_k$ .

In this study the energy dependence and nonlocality of the distorting potential as well as the finite-range effect in the  $(d, p)$  process are not discussed. Moreover, the breakup effect in the final channel is not taken into account. The findings summarized above therefore will need further investigation in view of these additional aspects. A more complete analysis will be very important.

## Acknowledgments

The authors thank K. Minomo and Y. S. Neoh for fruitful discussions. The numerical calculation was carried out with the computer facilities at the Research Center for Nuclear Physics, Osaka University. This work was supported in part by Grants-in-Aid of the Japan Society for the Promotion of Science (Grants No. JP15J01392 and No. JP25400255) and by the ImPACT Program of the Council for Science, Technology and Innovation (Cabinet Office, Government of Japan).

- 
- [1] K. L. Jones *et al.*, *Nature (London)* **465**, 454 (2010).
  - [2] K. L. Jones *et al.*, *Phys. Rev. C* **84**, 034601 (2011).
  - [3] J. Lee *et al.*, *Phys. Rev. C* **83**, 014606 (2011).
  - [4] S. D. Pain *et al.*, *Phys. Rev. Lett.* **114**, 212501 (2015).
  - [5] V. Margerin *et al.*, *Phys. Rev. Lett.* **115**, 062701 (2015).
  - [6] R. C. Johnson and P. J. R. Soper, *Phys. Rev. C* **1**, 976 (1970).
  - [7] R. C. Johnson and P. C. Tandy, *Nucl. Phys. A* **235**, 56 (1974).
  - [8] N. K. Timofeyuk and R. C. Johnson, *Phys. Rev. C* **59**, 1545 (1999).
  - [9] F. Delaunay, F. M. Nunes, W. G. Lynch, and M. B. Tsang, *Phys. Rev. C* **72**, 014610 (2005).
  - [10] A. M. Moro, F. M. Nunes, and R. C. Johnson, *Phys. Rev. C* **80**, 064606 (2009).
  - [11] A. M. Mukhamedzhanov, D. Y. Pang, C. A. Bertulani, and A. S. Kadyrov, *Phys. Rev. C* **90**, 034604 (2014).
  - [12] T. Fukui, K. Ogata, and M. Yahiro, *Phys. Rev. C* **91**, 014604 (2015).
  - [13] L. D. Faddeev, *Zh. Eksp. Theor. Fiz.* **39**, 1459 (1960) [*Sov. Phys. JETP* **12**, 1014 (1961)].
  - [14] E. O. Alt, P. Grassberger, and W. Sandhas, *Nucl. Phys. B* **2**, 167 (1967).
  - [15] A. Deltuva and A. C. Fonseca, *Phys. Rev. C* **79**, 014606 (2009).
  - [16] A. Deltuva, *Phys. Rev. C* **79**, 021602 (2009).
  - [17] A. Deltuva, A. Ross, E. Norvaisas, and F. M. Nunes, *Phys. Rev. C* **94**, 044613 (2016).
  - [18] N. K. Timofeyuk and R. C. Johnson, *Phys. Rev. Lett.* **110**, 112501 (2013).
  - [19] N. K. Timofeyuk and R. C. Johnson, *Phys. Rev. C* **87**, 064610 (2013).
  - [20] R. C. Johnson and N. K. Timofeyuk, *Phys. Rev. C* **89**, 024605 (2014).
  - [21] G. W. Bailey, N. K. Timofeyuk, and J. A. Tostevin, *Phys. Rev. Lett.* **117**, 162502 (2016).
  - [22] M. Kamimura, M. Yahiro, Y. Iseri, Y. Sakuragi, H. Kameyama, and M. Kawai, *Prog. Theor. Phys. Suppl.* **89**, 1 (1986).
  - [23] N. Austern, Y. Iseri, M. Kamimura, M. Kawai, G. Rawitscher, and M. Yahiro, *Phys. Rep.* **154**, 125 (1987).
  - [24] M. Yahiro, K. Ogata, T. Matsumoto, and K. Minomo, *Prog. Theor. Exp. Phys.* **2012**, 01A206 (2012).
  - [25] F. M. Nunes and A. Deltuva, *Phys. Rev. C* **84**, 034607 (2011).
  - [26] N. J. Upadhyay, A. Deltuva, and F. M. Nunes, *Phys. Rev. C* **85**, 054621 (2012).
  - [27] D. Y. Pang and A. M. Mukhamedzhanov, *Phys. Rev. C* **90**, 044611 (2014).
  - [28] K. Ogata and K. Yoshida, *Phys. Rev. C* **94**, 051603(R) (2016).
  - [29] N. Austern, M. Yahiro, and M. Kawai, *Phys. Rev. Lett.* **63**, 2649 (1989).
  - [30] N. Austern, M. Kawai, and M. Yahiro, *Phys. Rev. C* **53**, 314 (1996).
  - [31] M.C. Birse and E. F. Redish, *Nucl. Phys. A* **406**, 149 (1982).
  - [32] A. Bohr and B. R. Mottelson, *Nuclear Structure* (Benjamin, New York, 1969), Vol. I.
  - [33] A. J. Koning and J. P. Delaroche, *Nucl. Phys. A* **713**, 231 (2003).
  - [34] T. Ohmura, B. Imanishi, M. Ichimura, and M. Kawai, *Prog. Theor. Phys.* **43**, 347 (1970).
  - [35] See the ancillary file for the angular distribution of the  $(d, p)$  cross sections for the 128 systems calculated with CDCC, CDCC-AD, and CDCC without the closed channels.
  - [36] G. R. Satchler, *Direct Nuclear Reactions*, (Clarendon Press, Oxford, 1983).
  - [37] K. Hatanaka, *et al.*, *Phys. Rev. Lett.* **78** (1997) 1014.
  - [38] T. Noro, *et al.*, Proceedings of the RCNP International Symposium on Nuclear Responses and Medium Effects, Osaka, 1998, Universal Academy Press, Tokyo, p. 167 (1998).